We are IntechOpen,
the world's leading publisher of
Open Access books
Built by scientists, for scientists

4,800
Open access books available

122,000
International authors and editors

135M
Downloads

Our authors are among the

154
Countries delivered to

TOP 1%
most cited scientists

12.2%
Contributors from top 500 universities

CLARIVATE ANALYTICS
BOOK CITATION INDEX
INDEXED

WEB OF SCIENCE™

Selection of our books indexed in the Book Citation Index
in Web of Science™ Core Collection (BKCI)

Interested in publishing with us?
Contact book.department@intechopen.com

Numbers displayed above are based on latest data collected.
For more information visit www.intechopen.com

Analogue of the Event Horizon in Fibers

Friedrich König, Thomas G. Philbin, Chris Kuklewicz, Scott Robertson,
Stephen Hill, and Ulf Leonhardt
School of Physics and Astronomy, University of St Andrews, North Haugh,
St Andrews, Fife, KY16 9SS
United Kingdom

1. Introduction

In 1974 Stephen Hawking predicted that gravitational black holes would emit thermal radiation and decay (Hawking, 1974). This radiation, emitted from an area called the event horizon, is since known as Hawking radiation. To date it is still one of the most intriguing physical effects and bears great importance for the development of a quantum theory of gravity, cosmology and high energy physics.

The Hawking effect is one of a rich class of quantum properties of the vacuum (Birrell & Davies, 1984; Brout et. al., a; Milonni, 1994). For example, in the Unruh effect (Moore, 1970; Fulling, 1973; Davies, 1975; DeWitt, 1975; Unruh, 1976), an accelerated observer perceives the Minkowski vacuum as a thermal field. The physics of Hawking radiation leaves us with fascinating questions about the laws of nature at transplanckian scales, the conservation of information and physics beyond the standard model. Because of the thermal nature of the radiation, it is characterized by a temperature, the Hawking temperature. For stable astronomical black holes this lies far below the temperature of the cosmic microwave background, such that an observation of Hawking radiation in astrophysics seems unlikely.

Laboratory analogues of black holes have the potential to make the effect observable (Unruh, 1981; Schleich & Scully, 1984). The space-time geometry of the gravitational field can be represented in coordinates that act as an effective flow (Novello et al., 2002; Volovik, 2003; Unruh, 1981; Jacobson, 1991; Rousseaux et al., 2008). The event horizon lies where the flow velocity appears to exceed the speed of light in vacuum. Analogue systems are thus inspired by the following intuitive idea (Unruh, 1981): the black hole resembles a river (Jacobson, 1991; Rousseaux et al., 2008), a moving medium flowing towards a waterfall, the singularity. Imagine that the river carries waves propagating against the current with speed c'. The waves play the role of light where c' represents c, the speed of light in vacuum. Suppose that the closer the river gets to the waterfall the faster it flows and that at some point the speed of the river exceeds c'. Clearly, beyond this point no wave can propagate upstream anymore. The point of no return is the horizon.

In this chapter we are explaining a recent approach to the realization of an event horizon in optics (Philbin et. al, 2008). We start by describing the propagation of light in optical fibers and show the analogy to a curved space-time geometry. In Sec. 4 we quantize the field equation and give a Hamiltonian. Then we can use the geometrical optics approximation in Sec. 5 to find the behavior of light at a horizon, before we describe the scattering process that

is the analogue to Hawking radiation (Sec. 6). In Sec. 7 we describe the experimental findings of frequency shifts at the optical horizon and compare them to our predictions before we conclude.

2. Background

Nothing, not even light, can escape from a gravitational black hole. Yet according to quantum physics, the black hole is not entirely black, but emits waves in thermal equilibrium (Hawking, 1974; 1975; Birrell & Davies, 1984; Brout et. al. , a). The waves consist of correlated pairs of quanta, one originates from the inside and the other from the outside of the horizon. Seen from one side of the horizon, the gravitational black hole acts as a thermal black-body radiator sending out Hawking radiation (Hawking, 1974; 1975; Birrell & Davies, 1984; Brout et. al. , a). The effective temperature depends on the surface gravity (Hawking, 1974; 1975; Birrell & Davies, 1984; Brout et. al. , a) that, in our analogue model, corresponds to the flow-velocity gradient at the horizon (Novello et al., 2002; Volovik, 2003; Unruh, 1981; Jacobson, 1991).

Many systems have been proposed for laboratory demonstrations of analogues of Hawking radiation. One type of recent proposal (Garay et al., 2000; Giovanazzi et al., 2004; Giovanazzi, 2005) suggests the use of ultracold quantum gases such as alkali Bose-Einstein condensates or ultracold alkali Fermions (Giovanazzi, 2005). When a condensate in a waveguide is pushed over a potential barrier it may exceed the speed of sound (typically a few mm/s) and is calculated to generate a Hawking temperature of about 10nK (Giovanazzi et al., 2004). Helium-3 offers a multitude of analogues between quantum fluids and the standard model, including Einsteinian gravity (Volovik, 2003). For example, the analogy between gravity and surface waves in fluids (Schützhold & Unruh, 2002) has inspired ideas for artificial event horizons at the interface between two sliding superfluid phases (Volovik, 2002), but, so far, none of the quantum features of horizons has been measured in Helium-3. Proposals for optical black holes (Leonhardt & Piwnicki, 2000; Leonhardt, 2002) have relied on slowing down light (Milonni, 2004) such that it matches the speed of the medium (Leonhardt & Piwnicki, 2000) or on bringing light to a complete standstill (Leonhardt, 2002), but in these cases absorption may pose a severe problem near the horizon where the spectral transparency window (Milonni, 2004) vanishes.

But do we have to physically move the medium for establishing a horizon? Waves in the river may also see a horizon if the river depth changes due to some barrier, as the flow speed is increased above the barrier. There is again a black hole horizon just before the barrier. The situation is indistinguishable if the water of the river is at rest and the barrier is dragged along the river bed. Thus the medium can be locally disturbed and the wave speed can be reduced locally, leading to a situation of moving horizons in a medium at rest. Any Hawking radiation emitted this way will be immensely Doppler shifted to higher frequencies. Such ideas were discussed for moving solitons and domain walls (Jacobson & Volovik, 1998) in superfluid Helium-3 (Volovik, 2003) and more recently for microwave transmission lines with variable capacity (Schützhold & Unruh, 2005), but they have remained impractical so far.

Ultrashort optical pulses seem suited for this scenario as optical frequencies and velocities are very high. Moving a medium at a fraction of the speed of light seems illusive. The novel idea described in this chapter (Philbin et. al, 2008), illustrated in Fig. 1, is based on the nonlinear optics of ultrashort light pulses in optical fibers (Agrawal, 2001) where we exploit the remarkable control of the nonlinearity, birefringence and dispersion in microstructured fibers (Russell, 2003; Reeves et al., 2003). More recently, ultrashort laser pulse filamentation has been shown to exhibit asymptotic horizons based on similar principles (Faccio et al., 2009).
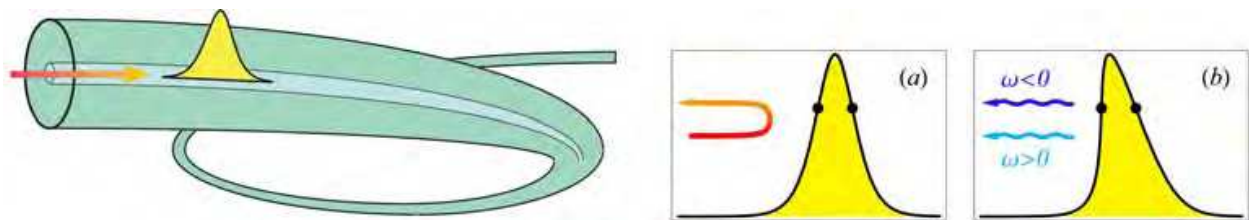
Fig. 1. Fiber-optical horizons. Left: a light pulse in a fiber slows down infrared probe light attempting to overtake it. Right: the diagrams are in the co-moving frame of the pulse. (a) Classical horizons. The probe is slowed down by the pulse until its group velocity matches the pulse speed at the points indicated in the figure, establishing a white hole at the back and a black hole at the front of the pulse. The probe light is blue-shifted at the white hole until the optical dispersion releases it from the horizon. (b) Quantum pairs. Even if no probe light is incident, the horizon emits photon pairs corresponding to waves of positive frequencies from the outside of the horizon paired with waves at negative frequencies from beyond the horizon. An optical shock has steepened the pulse edge, increasing the luminosity of the white hole (Philbin et. al, 2008).

3. Effective moving medium and metric

The fundamental idea behind the fiber-optical event horizon is the nonlinear and local modification of the refractive index of the fiber by a propagating pulse. As we will see later, this refractive index modification has to be ultrafast, i.e. the contributing nonlinearity is the optical Kerr effect (Agrawal, 2001): the (linear) effective refractive index of the fiber, n_0, gains an additional contribution δn that is proportional to the instantaneous pulse intensity I at position z and time t,

$$n = n_0 + \delta n, \quad \delta n \propto I(z,t). \tag{1}$$

This contribution to the effective refractive index n moves with the pulse. It acts as a local modification of the wave speed and thus as an effective moving medium, although nothing material is moving.

In what follows we will review how this nonlinearity arises in a fiber-waveguide, how it forms an effective moving medium, and that the fields follow a metric in analogy to a space-time manifold in the dispersionless case.

3.1 Waveguides

The waveguide confines light in the x and y direction and light propagates along the z direction. We assume a fiber homogeneous in z and with the Fourier-transformed susceptibility

$$\widetilde{\chi}_g = \widetilde{\chi}_g(\omega, x, y). \tag{2}$$

We represent the Fourier-transformed electric field strengths as

$$\widetilde{\mathbf{E}}(\omega, \mathbf{r}) = \widetilde{E}(\omega, z)\, \mathbf{U}(\omega, x, y), \tag{3}$$

where we assume linearly polarized light. Also we require that the fiber modes $\mathbf{U}$ are eigenfunctions of the transversal part of the wave equation for monochromatic light with eigenvalues $\beta^2(\omega)$,

$$\left(-\nabla \times (\nabla \times \mathbf{U}) + (1 + \tilde{\chi}_g)\frac{\omega^2}{c^2}\mathbf{U}\right) = \beta^2(\omega)\mathbf{U}. \tag{4}$$

For single-mode fibers, only one eigenvalue $\beta^2(\omega)$ exists.

The eigenvalues $\beta^2(\omega)$ of the transversal modes set the effective refractive indices $n(\omega)$ of the fiber for light pulses $E(t, z)$ defined by the relation

$$\beta = \frac{n(\omega)}{c}\omega. \tag{5}$$

In the absence of losses within the frequency range we are considering, the Fourier-transformed $\tilde{\chi}_g(\omega)$ in the longitudinal mode equation (4) is real for real ω and the longitudinal mode equation (4) is Hermitian and positive. Since the linear susceptibility $\chi_g(t)$ is real, $\tilde{\chi}_g(\omega)$ is an even function, which implies that $n^2(\omega)$ and $\beta^2(\omega)$ are even.

3.2 Effective moving medium

In our case, an intense ultrashort optical pulse interacts with a weak probe field, an incident wave of light or the vacuum fluctuations of the electromagnetic field itself (Milonni, 1994). The vacuum fluctuations are carried by modes that behave as weak classical light fields as well. The pulse is polarized along one of the eigen-polarizations of the fiber; the probe field may be co- or cross polarized. We assume that the intensity profile $I(z, t)$ of the pulse uniformly moves with constant velocity u during the interaction with the probe, neglecting the small deceleration due to the Raman effect and pulse distortions. Since the probe field is weak we can safely neglect its nonlinear interaction with the pulse or itself. As the intensity profile of the pulse is assumed to be fixed, we focus attention on the probe field. We describe the probe by the corresponding component A of the vector potential that generates the electric field E and the magnetic field B, with

$$E = -\partial_t A, \quad B = \partial_z A. \tag{6}$$

The probe field obeys the wave equation

$$(c^2\partial_z^2 + c^2\beta^2(i\partial_t) - \partial_t\chi\partial_t)A = 0, \quad \chi \propto I(z,t) \tag{7}$$

where χ denotes the susceptibility due to the Kerr effect of the pulse on the probe. β is given by Eq. (5) and we denote the effective refractive index by n_0. Equation (7) shows that the pulse indeed establishes an effective moving medium (Leonhardt, 2003). It is advantageous to use the retarded time τ and the propagation time ζ as coordinates, defined as

$$\tau = t - \frac{z}{u}, \quad \zeta = \frac{z}{u}, \tag{8}$$

because in this case the properties of the effective medium depend only on τ. τ and ζ play the roles of space and of time, respectively. The z and t derivatives are replaced by

$$\partial_t = \partial_\tau, \quad \partial_z = \frac{1}{u}(\partial_\zeta - \partial_\tau), \tag{9}$$

and the wave equation (7) becomes

$$(\partial_\zeta - \partial_\tau)^2 A = \partial_\tau \frac{u^2}{c^2} n^2 \partial_\tau A, \tag{10}$$

where the total refractive index n consists of the effective linear index n_0 and the Kerr contribution of the pulse,

$$n^2 = n_0^2 + \chi. \tag{11}$$

Since $\chi \ll n_0$ we approximate

$$n \approx n_0 + \delta n, \quad \delta n = \frac{\chi}{2n_0}, \tag{12}$$

where we can ignore the frequency dependance of n_0 in $\chi/(2n_0)$. Note that Eq. (8) does not describe a Lorentz transformation to an inertial system, but the τ and ζ are still valid coordinates.

3.3 Dispersionless case and metric

For simplicity, we consider the dispersionless case where the refractive index n_0 of the probe does not depend on the frequency. Note that a horizon inevitably violates this condition, because here light comes to a standstill, oscillating at increasingly shorter wavelengths, leaving any dispersionless frequency window. However, many of the essentials of horizons are still captured within the dispersionless model.

First, we can cast the wave equation (10) in a relativistic form, introducing a relativistic notation (Landau & Lifshitz, 1975) for the coordinates and their derivatives

$$x^\mu = (\zeta, \tau), \quad \partial_\mu = (\partial_\zeta, \partial_\tau) \tag{13}$$

and the matrix

$$g^{\mu\nu} = \begin{pmatrix} 1 & -1 \\ -1 & 1 - u^2 n^2/c^2 \end{pmatrix} \tag{14}$$

that resembles the inverse metric tensor of waves in moving fluids (Unruh, 1981; Visser, 1998). Adopting these definitions and Einstein's summation convention over repeated indices the wave equation (10) appears as

$$\partial_\mu g^{\mu\nu} \partial_\nu A = 0, \tag{15}$$

which is almost the free wave equation in a curved space-time geometry (Landau & Lifshitz, 1975) (In the case of a constant refractive index the analogy between the moving medium and a space-time manifold is perfect[1].). The effective metric tensor $g_{\mu\nu}$ is the inverse of $g^{\mu\nu}$ (Landau & Lifshitz, 1975). We obtain

---

[1] The exact wave equation in a curved space time geometry is $\partial_\mu \sqrt{-g} g^{\mu\nu} \partial_\nu A = 0$. where g is the determinant of the metric tensor (Landau & Lifshitz, 1975). In the case (14) g depends only on the refractive index n and hence g is constant for constant n.

$$g_{\mu\nu} = \frac{c^2}{n^2 u^2} \begin{pmatrix} u^2 n^2/c^2 - 1 & -1 \\ -1 & -1 \end{pmatrix}. \tag{16}$$

In subluminal regions where the velocity c/n of the probe light exceeds the speed of the effective medium, *i.e.* the velocity u of the pulse, the measure of time $u^2 n^2/c^2 - 1$ in the metric (16) is negative. Here both ∂_τ and ∂_ζ are timelike vectors (Landau & Lifshitz, 1975). In superluminal regions, however, c/n is reduced such that $u^2 n^2/c^2 - 1$ is positive. A horizon, where time stands still, is established where the velocity of light matches the speed of the pulse.

4. Lagrangian formulation and Hamiltonian

We have now seen that the probe is interacting within an effective moving medium in a way similar to waves in moving fluids, mimicking space-time in general relativity. To find the classical as well as quantum mechanical evolution of the field, we will next find a suitable Lagrangian density and the canonical Hamiltonian. Then we expand the quantized vector potential in terms of creation and annihilation operators.

4.1 Action
The theory of quantum fields at horizons (Hawking, 1974; 1975; Birrell & Davies, 1984; Brout et. al. , a) predicts the spontaneous generation of particles. The quantum theory of light in dielectric media at rest has reached a significant level of sophistication (See e.g. Knöll et. al., 2001), because it forms the foundation of quantum optics (Leonhardt, 2003; See e.g. U. Leonhardt, 1993), but quantum light in moving media is much less studied (Leonhardt, 2003). In optical fibers, light is subject to dispersion, which represents experimental opportunities and theoretical challenges: we should quantize a field described by a classical wave equation of high order in the retarded time. Moreover, strictly speaking, dispersion is always accompanied by dissipation, which results in additional quantum fluctuations (See e.g. Knöll et. al., 2001). Here, however, we assume to operate in frequency windows where the absorption is negligible. To deduce the starting point of the theory, we begin with the dispersionless case in classical optics and then proceed to consider optical dispersion for light quanta.

The classical wave equation of one-dimensional light propagation in dispersionless media follows from the Principle of Least Action (Landau & Lifshitz, 1975) with the action of the electromagnetic field in SI units

$$\begin{aligned} S &= \int\int \frac{\varepsilon_0}{2} \left(n^2 E^2 - c^2 B^2 \right) dz\,dt \\ &= \int\int \frac{\varepsilon_0}{2} \left[-A\partial_\tau n^2 \partial_\tau A - c^2 (\partial_z A)^2 \right] u\,d\tau\,d\zeta \end{aligned} \tag{17}$$

and hence the Lagrangian density

$$\mathscr{L} = -\frac{\varepsilon_0}{2} \left[A\partial_\tau n^2 \partial_\tau A + c^2 (\partial_z A)^2 \right]. \tag{18}$$

In order to include the optical dispersion in the fiber and the effect of the moving pulse, we express the refractive index in terms of $\beta(\omega)$ and the effective susceptibility $\chi(\tau)$ caused by the pulse, using Eqs. (5) and (11) with $\omega = i\partial_\tau$. We thus propose the Lagrangian density

$$\mathcal{L} = \frac{\varepsilon_0}{2} \left[A \left(c^2 \beta^2 (i\partial_\tau) - \partial_\tau \chi \partial_\tau \right) A - c^2 (\partial_z A)^2 \right]. \tag{19}$$

In the absence of losses, $\beta^2(\omega)$ is an even function (Sec. 3.1). We write down the Euler-Lagrange equation (Landau & Lifshitz, 1975) for this case

$$\partial_\zeta \frac{\partial \mathcal{L}}{\partial (\partial_\zeta A)} - \sum_{\nu=0}^{\infty} (-1)^\nu \partial_\tau^\nu \frac{\partial \mathcal{L}}{\partial (\partial_\tau^\nu A)} = 0 \tag{20}$$

and obtain the wave equation (10). Thus the Lagrangian density (19) is correct.

4.2 Quantum field theory

According to the quantum theory of fields (Weinberg, 1999) the component A of the vector potential is described by an operator $\hat{A}$. Since the classical field A is real, the operator $\hat{A}$ must be Hermitian. For finding the dynamics of the quantum field we quantize the classical relationship between the field, the canonical momentum density and the Hamiltonian: we replace the Poisson bracket between the field A and the momentum density $\partial \mathcal{L}/\partial(\partial_\zeta A)$ by the fundamental commutator between the quantum field $\hat{A}$ and the quantized momentum density (Weinberg, 1999). We obtain from the Lagrangian (19) the canonical momentum density

$$\hat{\pi} = -\varepsilon_0 \frac{c^2}{u} \partial_z \hat{A} \tag{21}$$

and postulate the equivalent of the standard equal-time commutation relation (Weinberg, 1999; Mandel &Wolf, 1995)

$$\left[\hat{A}(\zeta, \tau_1), \hat{\pi}(\zeta, \tau_2) \right] = \frac{i\hbar}{u} \delta(\tau_1 - \tau_2). \tag{22}$$

We obtain the Hamiltonian

$$\begin{aligned}
\hat{H} &= \int \left(\hat{\pi} \partial_\zeta \hat{A} - \mathcal{L} \right) u \, d\tau \\
&= \frac{\varepsilon_0}{2} \int \left(\frac{c^2}{u^2} \left((\partial_\tau \hat{A})^2 - (\partial_\zeta \hat{A})^2 \right) - \hat{A} \left(c^2 \beta^2 - \partial_\tau \chi \partial_\tau \right) \hat{A} \right) u \, d\tau.
\end{aligned} \tag{23}$$

One verifies that the Heisenberg equation of the quantum field $\hat{A}$ is the classical wave equation (10), as we would expect for fields that obey linear field equations.

4.3 Mode expansion

Since the field equation is linear and classical, we represent $\hat{A}$ as a superposition of a complete set of classical modes multiplied by quantum amplitudes $\hat{a}_k$. The mode expansion is Hermitian for a real field such as the electromagnetic field,

$$\hat{A} = \sum_k \left(A_k \hat{a}_k + A_k^* \hat{a}_k^\dagger \right). \tag{24}$$

The modes A_k obey the classical wave equation (15) and are subject to the orthonormality relations (Birrell & Davies, 1984; Brout et. al., a; Leonhardt, 2003)

$$(A_k, A_{k'}) = \delta_{kk'} \quad (A_k^*, A_{k'}) = 0 \tag{25}$$

with respect to the scalar product

$$(A_1, A_2) = \frac{\varepsilon_0 c^2}{i\hbar} \int (A_1^* \partial_z A_2 - A_2 \partial_z A_1^*) d\tau. \tag{26}$$

The scalar product is chosen such that it is a conserved quantity for any two solutions A_1 and A_2 of the classical wave equation (10),

$$\partial_\zeta (A_1, A_2) = 0, \tag{27}$$

with a prefactor to make the commutation relations between the mode operators particularly simple and transparent. The scalar product serves to identify the quantum amplitudes $\hat{a}_k$ and $\hat{a}_k^\dagger$: the amplitude $\hat{a}_k$ belongs to modes A_k with positive norm, whereas the Hermitian conjugate $\hat{a}_k^\dagger$ is the quantum amplitude to modes A_k^* with negative norm, because

$$(A_1^*, A_2^*) = -(A_1, A_2). \tag{28}$$

Using the orthonormality relations (25) we can express the mode operators $\hat{a}_k$ and $\hat{a}_k^\dagger$ as projections of the quantum field $\hat{A}$ onto the modes A_k and A_k^* with respect to the scalar product (26),

$$\hat{a}_k = (A_k, \hat{A}), \quad \hat{a}_k^\dagger = -(A_k^*, \hat{A}). \tag{29}$$

We obtain from the fundamental commutator (22) and the orthonormality relations (25) of the modes the Bose commutation relations

$$[\hat{a}_k, \hat{a}_{k'}^\dagger] = \delta_{kk'}, \quad [\hat{a}_k, \hat{a}_{k'}] = 0. \tag{30}$$

Therefore light consists of bosons and the quantum amplitudes $\hat{a}_k$ and $\hat{a}_k^\dagger$ serve as annihilation and creation operators.

The expansion (24) is valid for any orthonormal and complete set of modes. Consider stationary modes with frequencies ω_k' such that

$$\partial_\zeta A_k = -i\omega_k' A_k. \tag{31}$$

We substitute the mode expansion (24) in the Hamiltonian (23) and use the wave equation (10) and the orthonormality relations (25) to obtain

$$\hat{H} = \sum_k \hbar \omega_k' \left(\hat{a}_k^\dagger \hat{a}_k + \frac{1}{2} \right). \tag{32}$$

Each stationary mode contributes $\hbar \omega_k'$ to the total energy that also includes the vacuum energy. The modes with positive norm select the annihilation operators of a quantum field,

whereas the negative norm modes pick out the creation operators. In other words, the norm of the modes determines the particle aspects of the quantum field. In the Unruh effect (Moore, 1970; Fulling, 1973; Unruh, 1976; Davies, 1975; DeWitt, 1975), modes with positive norm consist of superpositions of positive and negative norm modes in the frame of an accelerated observer (Birrell & Davies, 1984; Brout et. al. , a). Consequently, this observer perceives the Minkowski vacuum as thermal radiation (Moore, 1970; Fulling, 1973; Unruh, 1976; Davies, 1975; DeWitt, 1975). In the Hawking effect (Hawking, 1974; 1975), the scattering of light at the event horizon turns out to mix positive and negative norm modes, giving rise to Hawking radiation.

5. Field evolution in the geometrical optics approximation

Here we will derive Hamilton's equations in the geometrical optics approximation to understand the frequency shifts of light near a horizon.
To quantitatively describe this effect, we will derive the frequency ω' in a co-moving frame that is connected to the laboratory-frame frequency ω by the Doppler formula

$$\omega' = \left(1 - \frac{nu}{c}\right)\omega. \tag{33}$$

For a stable pulse, ω' is a conserved quantity, whereas ω follows the contours of fixed ω' when δ_n varies with the intensity profile of the pulse, see Fig. 4. If δ_n becomes sufficiently large, the frequency ω completes an arch from the initial ω_1 to the final ω_2; it is blue-shifted by the white-hole horizon. At a black-hole horizon, the arch is traced the other way round from ω_2 to ω_1. For the frequency at the center of the arches an infinitesimal δ_n is sufficient to cause a frequency shift; at this frequency the group velocity of the probe matches the group-velocity of the pulse.

5.1 Geometrical optics

A moving dielectric medium with constant refractive index but nonuniform velocity appears to light exactly as an effective space-time geometry (Leonhardt, 2003)[2]. Since a stationary 1 + 1 dimensional geometry is conformally flat (Nakahara, 2003) a coordinate transformation can reduce the wave equation to describing wave propagation in a uniform medium, leading to plane-wave solutions (Leonhardt & Philbin, 2006). The plane waves appear as phase-modulated waves in the original frame. Consequently, in this case, geometrical optics is exact. In our case, geometrical optics provides an excellent approximation, because the variations of the refractive index are very small.
Consider a stationary mode A. We assume that the mode carries a slowly varying amplitude $\mathcal{A}$ and oscillates with a rapidly changing phase φ,

$$A = \mathcal{A}\exp(i\varphi). \tag{34}$$

We represent the phase as

$$\varphi = -\int \omega(\tau)\,d\tau - \omega'\zeta \tag{35}$$

---

[2] see footnote 1 in Sec. 3.3

and obtain from the wave equation (10) the dispersion relation

$$(\omega - \omega')^2 = \frac{u^2}{c^2} n^2 \omega^2 \tag{36}$$

by neglecting all derivatives of the amplitude $\mathcal{A}$. Here n includes the additional susceptibility χ due to the Kerr effect of the pulse according to Eq. (11). The dispersion relation has two sets of solutions describing waves that are co- or counter-propagating with the pulse in the laboratory frame. Counter-propagating waves will experience the pulse as a tiny transient change of the refractive index, whereas co-propagating modes may be profoundly affected.

Consider the solution given by Eq. (33). In this case, we obtain outside of the pulse in the laboratory frame $\varphi = n(\omega/c)z - \omega t$, which describes light propagating in the positive z direction. Consequently, the branch (33) of the dispersion relation corresponds to co-propagating light waves. We also see that ω is the frequency of light in the laboratory frame, whereas ω' is the frequency in the frame co-moving with the pulse. Equation (33) describes how the laboratory-frame and the co-moving frequencies are connected due to the Doppler effect.

In order to find the evolution of the amplitude $\mathcal{A}$, we substitute in the exact scalar product (26) the approximation (34) with the phase (35) and the dispersion relation (33). In the limit $\omega'_1 \to \omega'_2$ we obtain

$$(A_1, A_2) = \frac{2\varepsilon_0 c}{\hbar} \int \mathcal{A}^2 n\omega \exp\left(i\varphi_2 - i\varphi_1\right)d\tau, \tag{37}$$

which should give $\delta(\omega'_1 - \omega'_2)$ according to the normalization (25). The dominant, diverging contribution to this integral, generating the peak of the delta function, stems from $\tau \to \pm\infty$ (Landau & Lifshitz, 1977). Hence, for $\omega'_1 \to \omega'_2$, we replace φ in the integral by φ at $\tau \to \pm\infty$ where ω does not depend on τ anymore,

$$(A_1, A_2) = \frac{2\varepsilon_0 c}{\hbar} \int \mathcal{A}^2 n\omega \exp\left[i(\omega_2 - \omega_1)\tau\right]d\tau, \quad \omega_2 - \omega_1 = \frac{\partial\omega}{\partial\omega'}(\omega'_2 - \omega'_1), \tag{38}$$

which gives $\delta(\omega'_1 - \omega'_2)$ for

$$|\mathcal{A}|^2 = \frac{\hbar}{4\pi\varepsilon_0 c n\omega}\left|\frac{\partial\omega}{\partial\omega'}\right| \tag{39}$$

and positive frequencies ω in the laboratory frame. Note that positive frequencies ω' in the co-moving frame correspond to negative ω in superluminal regions where the pulse moves faster than the phase-velocity of the probe light.

Hamilton's equations (Landau & Lifshitz, 1976) determine the trajectories of light rays in the co-moving frame, parameterized by the pulse-propagation time ζ. Here τ plays the role of the ray's position. Comparing the phase (35) with the standard structure of the eikonal in geometrical optics (Born & Wolf, 1999) or the semiclassical wave function in quantum mechanics (Landau & Lifshitz, 1977) we notice that $-\omega$ plays the role of the conjugate momentum here. Therefore, we obtain Hamilton's equations with a different sign than usual (Landau & Lifshitz, 1976),

$$\dot{\tau} = -\frac{\partial \omega'}{\partial \omega}, \quad \dot{\omega} = \frac{\partial \omega'}{\partial \tau}. \tag{40}$$

Now we express $\dot{\tau}$ in terms of the group index in the laboratory frame. The group velocity v_g is the derivative of the frequency ω with respect to the wave number $n\omega/c$ (Agrawal, 2001)

$$n_g = n + \omega \frac{\partial n}{\partial \omega}. \tag{41}$$

We obtain from the first of Hamilton's equations (40) and the Doppler formula (33)

$$\dot{\tau} = \frac{u}{c} n_g - 1 = -\frac{n_g}{c} v_g', \quad v_g' = \frac{c}{n_g} - u \tag{42}$$

where v_g' denotes the difference between the group velocity of the probe v_g and the pulse speed u. We see that the velocity $\dot{\tau}$ in the co-moving frame (8) vanishes when the Kerr susceptibility χ reduces the group velocity c/n_g such that it matches the speed of the pulse u. Since $\dot{\omega}$ does not vanish here in general, the ray does not remain there, but changes direction in the co-moving frame.

At such a turning point we expect a violation of the validity of geometrical optics (Landau & Lifshitz, 1977). For example, the amplitude (39) would diverge here. Geometrical optics is an exponentially accurate approximation when

$$\left| \frac{\partial T}{\partial \tau} \right| \ll 1 \quad \text{for} \quad T = \frac{2\pi}{\omega}, \tag{43}$$

as we see from the analogy to the semiclassical approximation in quantum mechanics (Landau & Lifshitz, 1977). Here the cycle T plays the role of the wavelength. We get

$$\frac{\partial T}{\partial \tau} = \frac{\dot{\omega} T}{\omega \dot{\tau}}. \tag{44}$$

Consequently, geometrical optics indeed is no longer valid near a turning point where

$$n_g = \frac{c}{u} \quad v_g' = v_g \frac{\partial \omega'}{\partial \omega} = 0. \tag{45}$$

This turning point defines a *group velocity horizon* where the pulse has slowed down the probe such that it matches the speed of the pulse. At this horizon the incident mode is converted into a mode that represents another solution of the dispersion relation; a red-or blue-shifted wave, depending on the dispersion and the sign of the first derivative of χ with respect to τ at the group velocity horizon. White holes correspond to increasing χ and black holes to decreasing χ. White holes blue-shift, because incident waves freeze in front of the horizon, oscillating with increasing frequency. Black holes red-shift, because they stretch any emerging waves (also because black holes are time-reversed white holes). Due to the dispersion of the fiber, the refractive index changes with frequency. In turn, the dispersion limits the frequency shifting by tuning the light out of the grip of the horizon. In particular, the dispersion limits the blue-shifting at white-hole horizons to respectable but finite frequencies, considering the tiny magnitude of χ, as we discuss in Sec. 7.1.

At the event horizons of astrophysical black holes, similar effects are expected (t'Hooft, 1985; Jacobson, 1991) when, due to the wave-number divergence, the wavelength of light is reduced below the Planck length scale $\sqrt{hG/c^3}$ where G is the gravitational constant. The physics beyond the Planck scale is unknown. This trans-Planckian physics should regularize the logarithmic phase singularities (Birrell & Davies, 1984; Brout et. al. , a) of modes at the event horizon. Studies of trans-Planckian physics indicate, that the Hawking effect of the black hole is not affected (Unruh, 1995; Brout et al. , b). On the other hand, the quantum radiation of white holes is dominated by trans-Planckian physics, because of the extreme blue shift at white-hole horizons. It has been predicted (Corley & Jacobson, 1999; Leonhardt & Philbin, 2007) that black-hole white-hole pairs could act as black hole lasers in a regime of anomalous group velocity dispersion. From a theoretical point of view, trans-Planckian physics regularizes some of the arcane features of quantum black holes and gives a more natural picture of the physics behind the Hawking effect (Brout et al. , b). In our case, the optical analogue of trans-Planckian physics, optical dispersion, is known in principle and turns out to be to the advantage of the experiment.

6. Hawking effect

Imagine instead of a single probe mode a set of probe modes. The modes should be sufficiently weakly excited such that they do not interact with each other, but they experience the cross Kerr effect of the pulse, the presence of the medium (1) moving with the velocity u. Themodes constitute a quantum field of light in a moving medium (Leonhardt, 2003).
A *phase-velocity horizon* is formed if the pulse has slowed down the probe such that its phase velocity is lower than the speed of the pulse. The condition for this horizon is:

$$\frac{\omega'}{\omega} = 0. \tag{46}$$

Here an additional effect occurs: the spontaneous creation of photon pairs, Hawking radiation. In the near ultraviolet around $\lambda = 300$nm, the dispersion of fibers is dominated by the bare dispersion of glass where $n_0(\omega)$ rapidly grows with frequency (Agrawal, 2001), exceeding the group index c/u of the pulse. For such ultraviolet modes, the pulse moves at superluminal speed. According to the Doppler formula (33) these superluminal modes oscillate with negative frequencies ω' in the co-moving frame for positive frequencies ω in the laboratory frame, and vice versa. Moreover, each subluminal mode with positive ω has a superluminal partner oscillating at the same co-moving frequency ω', but with negative laboratory frequency, see Fig. 2. The Kerr susceptibility of the pulse may slow down the subluminal modes such that the pulse moves at superluminal speed. As we will show in this section, in this case suband superluminal modes are partially converted into each other and photon pairs are created, even if the modes were initially in their vacuum states (Birrell & Davies, 1984; Brout et. al., a). This process is the optical analogue of Hawking radiation (Hawking, 1974; 1975). Photons with positive ω' correspond to the particles created at the outside of the black hole (Birrell & Davies, 1984; Brout et. al., a), while the negative-frequency photons represent their partners beyond the horizon.
In the fiber-optical case, the photon pairs are distinguishable from the intense pulse, because their frequencies differ by an octave. Furthermore, one can discriminate the Hawking effect
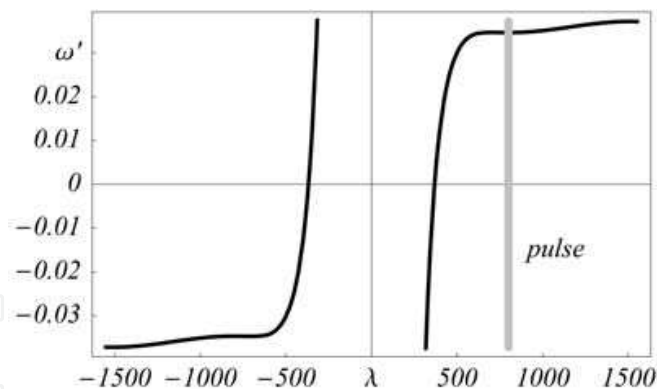
Fig. 2. Doppler-shifted frequency versus wavelength (Philbin et. al, 2008). The figure shows the co-moving frequency (33) (in 10^{15}Hz) for the micro-structured fiber versus the wavelength λ (in nm). We used the fiber dispersion data in Eq. (72), apart from two constants that we fitted to the Sellmeier formula for fused silica at short wavelengths (Agrawal, 2001).

from other nonlinear optical processes, such as Four-Wave Mixing, because it is not subject to their phase-matching conditions (Agrawal, 2001). Moreover, in addition to observing Hawking radiation *per se*, one could detect the correlations of the Hawking partners — a feat that is utterly impossible in astrophysics, because there the partner particles are lost beyond the horizon of the black hole.

Thus in this section we investigate the scattering mechanism which leads to Hawking radiation for our analogue system in a classical as well as quantized treatment.

6.1 Classical Hawking effect

For simplicity, we consider a single white-hole horizon, not the combination of black- and white-hole horizons generated by a moving pulse. We will argue later that in practice the white-hole will dominate the Hawking effect, which *a-posteriori* justifies this simplification. Suppose, without loss of generality, that at τ=0 the Kerr-reduced phase-velocity of the probe, c/n, matches the group velocity of the pulse u. We assume that the mode conversion occurs near this point and expand the Kerr susceptibility χ as a linear function in τ,

$$\chi(\tau) = \chi_h + \alpha''\tau, \quad \alpha'' = \left.\frac{\partial\chi}{\partial\tau}\right|_0. \tag{47}$$

The group velocity of the incident probe is much lower than the pulse speed u and so both the sub- and the superluminal probe travels from the front of the pulse to the back, from negative to positive retarded time τ. For a white-hole horizon χ increases for decreasing retarded time, and so $\dot{\chi}(0) < 0$.

We proceed similar to (Brout et al. , b) and focus on the conversion region where we Fourier-transform with respect to τ the wave equation (10) with the refractive index (11) for stationary waves in the co-moving frame and using the linear expansion (47). The frequency conjugate to τ is the laboratory-frame frequency ω. We replace τ by $-i\partial_\omega$, ∂_ζ by $-i\omega$ and ∂_τ by $-i\omega$, denote the Fourier-transformed vector potential by $\tilde{A}$, and obtain

$$\left(n_0^2 + \chi_h - i\alpha''\partial_\omega\right)\omega\tilde{A} = \left(1 - \frac{\omega'}{\omega}\right)^2 \frac{c^2}{u^2}\omega\tilde{A}. \tag{48}$$

This first-order equation has the exact solution

$$\tilde{A} = \frac{\tilde{\mathcal{A}}_0}{\omega} e^{-i\phi}, \quad \phi = -\frac{1}{\alpha''} \int \left[\left(1 - \frac{\omega'}{\omega}\right)^2 \frac{c^2}{u^2} - n_0^2 - \chi_h \right] d\omega \tag{49}$$

with constant $\tilde{\mathcal{A}}_0$. We introduce

$$\alpha' \equiv -\frac{u^2}{c^2} \frac{\alpha''}{2} \approx -\frac{u}{c} \frac{\dot{\chi}(0)}{2n_0} = -\frac{u}{c} \frac{\partial n}{\partial \tau}\bigg|_0. \tag{50}$$

Note that the phase ϕ contains a logarithmic contribution,

$$\phi = -\frac{\omega'}{\alpha'} \ln \omega + \phi_0(\omega). \tag{51}$$

This logarithmic asymptotics of the phase will lead to the characteristic mode conversion at the phase velocity horizon. In order to see this, we Fourier-transform $\tilde{A}$ back to the domain of the retarded time,

$$A = \int_{-\infty}^{+\infty} \tilde{A} e^{-i\omega\tau} d\omega = \int_{-\infty}^{+\infty} \frac{\tilde{\mathcal{A}}_0}{\omega} e^{-i\phi - i\omega\tau} d\omega \tag{52}$$

and use the saddle-point approximation, *i.e.* we quadratically expand the phase $\phi + \omega\tau$ around the stationary points where $\partial_\omega(\phi + \omega\tau)$ vanishes and perform the integration as Gaussian integrals along the direction of steepest descent. One easily verifies that the stationary points are the solutions of the dispersion relation (36). We denote the two solutions by $\omega_\pm$ indicating their sign. We obtain for the second derivative in the quadratic expansion

$$\partial_\omega^2(\phi + \omega\tau) = -\frac{2}{\dot{\chi}(0)} \frac{n}{\omega} \left(\frac{c}{u} - n_g\right). \tag{53}$$

The Gaussian integrals at $\omega_\pm$ are proportional to the inverse square root of $\partial_\omega^2(\phi + \omega\tau)$. We see from Eqs. (40) and (42) that they are consistent with the amplitudes (39) of geometrical optics. Consequently, we obtain a superposition of the two waves (34) that correspond to the two physically-relevant branches of the dispersion relation (36). We denote the positive-frequency wave by A_+ and the negative-frequency component by A_-^*. The star indicates that this component resembles the complex conjugate of a mode, because a mode predominantly contains positive laboratory-frame frequencies, according to the normalization (39). The coefficient of A_-^* is given by the exponential of the phase integral from the positive branch ω_+ to the negative frequency ω_- on the complex plane. The amplitude of the coefficient is the exponent of the imaginary part of the phase integral, while the phase of the coefficient is given by the real part. We can incorporate the phase of the superposition coefficient in the prefactor (39), but not the amplitude. The imaginary part of the phase integral comes from the logarithmic term (51), giving $\pi\omega'/\alpha'$. Therefore, the relative weight of the negative-frequency component in the converted mode is $\exp(-\pi\omega'/\alpha')$. We thus obtain for $\tau < 0$

$$A \sim Z^{1/2} \left(A_+ + A_-^* e^{-\pi\omega'/\alpha'} \right) \tag{54}$$

where Z denotes a constant for given ω'. We determine the physical meaning of Z in Sec. 6.2, but here we can already work out its value by the following procedure: consider a wavepacket with co-moving frequencies around ω' that crosses the horizon. Suppose that this wavepacket is normalized to unity. After having crossed the horizon, the norm of the positive-frequency component is Z, while the negative-frequency component has the negative norm $-Z\exp(-2\pi\omega'/\alpha')$. The sum of the two components must give unity, and so

$$Z = \left(1 - e^{-2\pi\omega'/\alpha'} \right)^{-1}. \tag{55}$$

We represent $Z^{1/2}$ as $\cosh\xi$ and obtain from Eq. (55)

$$Z^{1/2} = \cosh\xi, \quad Z^{1/2} e^{-\pi\omega'/\alpha'} = \sinh\xi. \tag{56}$$

Consequently, the incident wave $A_\pm$ is converted into the superposition $A_\pm \cosh\xi + A_\mp^* \sinh\xi$ when it crosses the horizon from positive to negative τ. Hence we obtain for this process the mode

$$A_{\pm\text{in}} \sim \begin{cases} A_\pm & : \quad \tau > 0 \\ A_\pm \cosh\xi + A_\mp^* \sinh\xi & : \quad \tau < 0 \end{cases}. \tag{57}$$

Equation (57) describes the fate of a classical wave that crosses the horizon. A negative-frequency component is generated with weight $\sinh^2 \xi$ relative to the initial wave, but, since $\cosh\xi > 1$, the positive-frequency wave has been amplified. The mode conversion at the horizon is thus an unusual scattering process where the concerted modes are amplified, at the expense of the energy of the driving mechanism, the pulse in our case. (It is also mathematically unusual — the Hawking effect corresponds to scattering without turning points in the complex plane.) Wherever there is amplification of classical waves, *i.e.* stimulated emission of waves, there also is spontaneous emission of quanta (Caves, 1982) — in the case of horizons, Hawking radiation.

6.2 Hawking radiation

Suppose that no classical probe light is incident; the modes $A_{\pm\text{in}}$ are in the vacuum state. The incident modes are characterized by the asymptotics $A_\pm$ for $\tau > 0$ while outgoing modes are required to approach $A_\pm$ for $\tau < 0$. We perform the superposition

$$A_{\pm\text{out}} = A_{\pm\text{in}} \cosh\xi - A_{\mp\text{in}}^* \sinh\xi \tag{58}$$

and see that $A_{\pm\text{out}}$ obeys the asymptotics

$$A_{\pm\text{out}} \sim \begin{cases} A_\pm \cosh\xi - A_\mp^* \sinh\xi & : \quad \tau > 0 \\ A_\pm & : \quad \tau < 0 \end{cases}, \tag{59}$$

as required for outgoing modes. The modes (57) and (58) describe two sets of mode expansions (24) of one and the same quantum field; for a given ω' the sum of $A_{\pm\text{in}} \hat{a}_{\pm\text{in}}$ and

$A^*_{\pm\text{in}}\hat{a}^\dagger_{\pm\text{in}}$ over the two signs $\pm$ of ω must give the corresponding sum of $A_{\pm\text{out}}\hat{a}_{\pm\text{out}}$ and $A^*_{\pm\text{out}}\hat{a}^\dagger_{\pm\text{out}}$. Consequently,

$$\hat{a}_{\pm\text{in}} = \hat{a}_{\pm\text{out}}\cosh\zeta - \hat{a}^\dagger_{\mp\text{out}}\sinh\zeta \tag{60}$$

and by inversion

$$\hat{a}_{\pm\text{out}} = \hat{a}_{\pm\text{in}}\cosh\zeta + \hat{a}^\dagger_{\mp\text{in}}\sinh\zeta. \tag{61}$$

The vacuum state $|\text{vac}\rangle$ of the incident field is the eigenstate of the annihilation operators $\hat{a}_{\pm\text{in}}$ with zero eigenvalue (the state that the $\hat{a}_{\pm\text{in}}$ annihilate),

$$\hat{a}_{\pm\text{in}}|\text{vac}\rangle = 0. \tag{62}$$

To find out whether and how many quanta are spontaneously emitted by the horizon, we express the in-coming vacuum in terms of the out-going modes. We denote the out-going photon-number eigenstates, the out-going Fock states (Leonhardt, 2003), by $|n_+,n_-\rangle$ with the integers $n_\pm$. Using the standard relations for the annihilation and creation operators

$$\hat{a}|n\rangle = \sqrt{n}|n-1\rangle, \quad \hat{a}^\dagger|n\rangle = \sqrt{n+1}|n+1\rangle, \tag{63}$$

one verifies that $\hat{a}_{\pm\text{in}}$ vanishes for the state

$$|\text{vac}\rangle = Z^{-1/2}\sum_{n=0}^{\infty} e^{-n\pi\omega'/\alpha'}|n,n\rangle. \tag{64}$$

This is the remarkable result obtained by Hawking (Hawking, 1974; 1975) for the horizon of the black hole. First, it shows that the event horizon spontaneously generates radiation from the incident quantum vacuum. Second, the emitted radiation consists of correlated photon pairs, each photon on one side is correlated to a partner photon on the other side, because they are always produced in pairs. The total quantum state turns out to be an Einstein-Podolski-Rosen state (Leonhardt, 2003), the strongest entangled state for a given energy (Barnett & Phoenix, 1989; 1991). Third, light on either side of the horizon consists of an ensemble of photon-number eigenstates with probability $Z^{-1}e^{-2n\pi\omega'/\alpha'}$. This is a Boltzmann distribution of n photons with energies $n\hbar\omega$. Consequently, the horizon emits a Planck spectrum of blackbody radiation with the Hawking temperature of (Philbin et. al, 2008):

$$T' = \frac{\hbar\alpha'}{2\pi k_B}, \tag{65}$$

where k_B denotes Boltzmann's constant. Fourth, this Planck spectrum is consistent with Bekenstein's black-hole thermodynamics (Bekenstein, 1973): black holes seem to have an entropy and a temperature.
In our case, the spectrum of the emitted quanta is a Planck spectrum for the frequencies ω in the co-moving frame, as long as a phase-velocity horizon exists. We performed our analysis for the white-hole horizon, but, since black holes are time-reversed white holes, we

arrive at the same result for the black hole, except that the roles of the incident and outgoing modes are reversed. In the laboratory frame, the spectrum is given by the dependance of ω' on the laboratory frequency ω outside of the pulse, *i.e.* by the dispersion relation (33) for $\chi = 0$. In our case, $\omega(\omega')$ is single-valued for the spectral region where phase-velocity horizons are established, see Fig. 2, and so the spectra of black- and white-hole horizons are identical for identical α'. For evaluating α' we consider δn at $\tau = 0$, where

$$\alpha' = -\frac{u}{c}\frac{\partial n}{\partial \tau}\bigg|_0 = -\frac{u}{c}\frac{\partial \delta n}{\partial \tau}\bigg|_0. \tag{66}$$

Note that T' denotes the Hawking temperature in the co-moving frame, defined with respect to the Doppler-shifted frequencies ω', a temperature that is characterized by the Doppler-shifted Hawking frequency α' in regions away from the pulse. We use the Doppler formula (33) with the refractive index (1) and the linearization (47) taken at $\tau = 0$, and obtain

$$\alpha' = \left(1 - n_0\frac{u}{c}\right)\alpha = \frac{u}{c}\delta n\bigg|_0 \alpha. \tag{67}$$

Consequently, the Hawking temperature T in the laboratory frame is

$$T = \frac{\hbar\alpha}{2\pi k_B}, \quad \alpha = -\frac{1}{\delta n}\frac{\partial \delta n}{\partial \tau}\bigg|_0. \tag{68}$$

T does not depend on the magnitude of δn, as long as a phase velocity horizon is established. Even the small refractive index variations of nonlinear-fiber optics (Agrawal, 2001) may lead to a substantial Hawking temperature when δn varies on the scale of an optical wavelength. Thus the particle-production rate depends primarily on the sharpness of the pulse. This important feature makes the experimental observation of Hawking radiation in optical fibers feasible, as modern few-cycle pulses are only a couple of wavelengths long (F. X. Kärtner, 2004; Brabez & Krausz, 2000). In addition, an optical shock can form and lead to significant further steepening of the trailing (white hole) edge of the pulse at the expense of the luminosity of the black hole (Agrawal, 2001; Philbin et. al, 2008). Assuming that the steepness of this shock front is comparable to twice the frequency of the pulse carrier, 8×10^{14}Hz, the Hawking temperature (68) reaches 10^3K, many orders of magnitude higher than condensed-matter analogues of the event horizon (Garay et al., 2000; Giovanazzi et al., 2004; Giovanazzi, 2005; Jacobson & Volovik, 1998).

7. Experiment

We will now describe the experimental observation of frequency shifting of light at the group velocity horizon. Based on the theory of Secs. 3 - 6, we also derive mathematical expressions for the amount of blue shifting, for the spectral shape, and for estimating the efficiency of this process. We discuss the experimental proceedings and findings and compare them with the theory.

Soliton interactions in fibers are well studied. The connection to event horizons, however, had not been made and thus experiments merely focussed on related nonlinear effects such as optical pulse trapping in fibers (Efimov et al., 2005; Nishizawa & Goto, 2002; Gorbach & Skryabin, 2007; Hill et al., 2009) and pulse compression in fiber gratings (optical push

broom) (de Sterke, 1992; Steel et al., 1994; Broderick et al., 1997). The measurements described here for the first time focussed on the frequency shifts connected to analogues of the event horizon.

In order to observe the frequency shifts at the horizon we launch a pulse into the fiber to establish a group velocity horizon as explained in Sec. 5. We also launch a continuous wave of light, a probe, that follows the pulse with slightly higher group velocity, attempting to overtake it. The probe wavelength λ is chosen much longer than the pulse wavelength λ_0 in order to separate the two. While approaching the pulse, the Kerr contribution δ_n slows down the probe until the probe's group velocity reaches the speed of the pulse. The trailing end of the pulse establishes a white-hole horizon, an object that light cannot enter, unless it tunnels through the pulse. Conversely, the front end creates a black-hole horizon for probe light that is slower than the pulse. Since δ_n is small, the initial group velocity of the probe should be sufficiently close to the speed of the pulse.

In microstructured fibers (Russell, 2003) the group velocity dispersion can be engineered such that the group velocity of pulses of 800nm carrier wavelength matches the group velocities of probe light in the infrared around 1500nm. At the horizon of an astrophysical black hole light freezes, reaching wavelengths shorter than the Planck scale where the physics is unknown (The Planck length is given by $\sqrt{2\pi\hbar G/c^3}$ where G is the gravitational constant.) (t'Hooft, 1985; Jacobson, 1991). In our case, the fiber-optical analogue of Trans-Planckian physics is known and simple — it is contained in the frequency-dependance of the refractive index n, the dispersion of the fiber. At the trailing end of the pulse the incoming probe modes are compressed, oscillating with increasing frequency; they are blue-shifted. In turn, the dispersion limits the frequency shifting by tuning the probe out of the horizon. In the case of normal group-velocity dispersion the blue-shifted light falls behind.

7.1 Dispersion

The creation of artificial event horizons in optical fibers critically depends on the properties of these fibers. Microstructured fibers (Knight et. al., 1996; Russell, 2003) have an arrangement of holes close to the fiber core along the fiber. In the simplest picture, the holes lower the local refractive index in the transverse plane of the fiber, leading to substantially larger index variations compared to conventional fibers. In particular, the anomalous group velocity dispersion required for solitons can be generated at wavelengths reaching the visible. To create an artificial event horizon, an intense optical pulse has to be formed inside the fiber. Optical solitons (Hasegawa & Tappert, 1973; Mollenauer et al, 1980; Agrawal, 2001) offer a unique possibility for nondispersive stable pulses in fibers. These can be ultrashort, allowing for very high peak powers to drive the nonlinearity of the fiber.

The dispersion parameter D of optical fibers is defined as the change of group delay per wavelength change and fiber length. Its units are usually ps/(nmkm). Since the group delay per length is given by n_g/c and $n_g/c=\partial\beta/\partial\omega$, we have (Agrawal, 2001)

$$D = \frac{\partial}{\partial\lambda}\frac{n_g}{c} = \frac{\partial^2\beta}{\partial\lambda\partial\omega}, \quad \lambda = \frac{2\pi c}{\omega}. \tag{69}$$

The group velocity dispersion is often also characterized by β_2,

$$\beta_2 = \frac{\partial^2\beta}{\partial\omega^2} = -\frac{\lambda}{\omega}D. \tag{70}$$

The group velocity dispersion is normal for positive β_2 and negative D, and anomalous for negative β_2 and positive D.
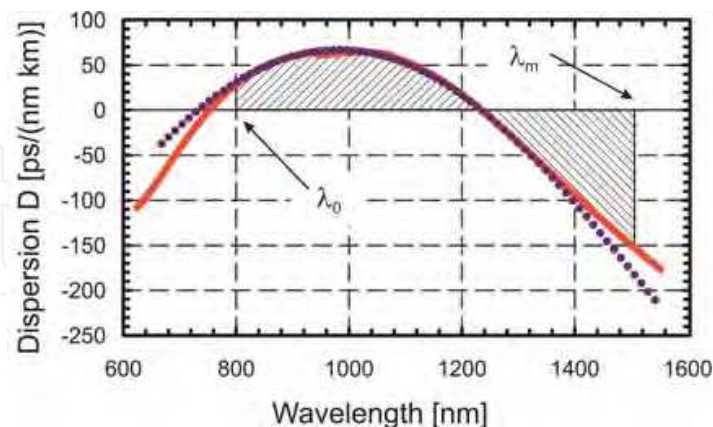

Fig. 3. Two measurements of the dispersion parameter D for the fiber used in the experiments (Philbin et. al, 2008). Red: technical specification; dotted: result of Alexander Podlipensky & Philip Russell, Max Planck Research Group in Optics, Information and Photonics, Erlangen, Germany. As the total shaded area vanishes, the two wavelengths at either end are group velocity matched.

For the creation of a horizon we chose a commercial microstructured fiber, model NL-PM-750B by Crystal Fiber A/S. Figure 3 shows the dispersion of the single mode fiber. The red curve is the manufacturer technical specification; the dotted line was measured for our particular fiber sample by Alexander Podlipensky and Philip Russell at the Max Planck Research Group in Optics, Information and Photonics in Erlangen, Germany. The fiber dispersion is anomalous between ≈ 740nm and ≈ 1235nm wavelength and normal otherwise. Further fiber properties are summarized in Table 1. Solitons can be created in this fiber using ultrashort pulses from Ti:Sapphire lasers. Light that would probe the horizon and experience blue shifting as a result, will have to be slowed down by the Kerr effect of the pulse such that its group velocity matches the speed u of the pulse. The Kerr nonlinearity is small, and so the initial group velocity of the probe should be only slightly higher than u. Integrating Eq. (69) we obtain

$$\int_{\lambda_0}^{\lambda} D \, d\lambda = \beta_1(\lambda) - \beta_1(\lambda_0) = \frac{1}{v_g(\lambda)} - \frac{1}{v_g(\lambda_0)}, \quad v_g(\lambda_0) = u. \tag{71}$$

Here λ_0 and λ denote the center wavelengths of the pulse and the probe light, respectively. Therefore, the probe light travels at the speed of the pulse if the integral of D vanishes, as illustrated by the shaded areas in Fig. 3. This probe wavelength is called the group velocity-matched wavelength λ_m (and ω_m the group velocity-matched frequency). For a pulse carrier-wavelength of 800nm and this fiber we obtain $\lambda_m \approx 1500$nm. This value of λ_m is useful and justifies the choice of fiber, because it is a standard wavelength for optical communication equipment and it is clearly separated from our spectrally broad pulses. Integrating Eq. (69) twice we obtain the propagation constant

$$\beta = \beta(\omega_0) + \frac{\omega - \omega_0}{u} + \int_{\omega_0}^{\omega} \int_{\lambda_0}^{\lambda} D \, d\lambda \, d\omega = n\frac{\omega}{c}, \tag{72}$$

where n is the linear effective refractive index of the fiber and ω_0 and ω denote the carrier frequency of pulse and probe, respectively.

In general, the two eigenmodes of polarization of the fiber have slightly different propagation constants β. This birefringence creates a refractive index difference Δn between the polarization modes. Our fiber exhibits strong birefringence Δn of a few times 10^{-4}. This leads to non-negligible changes in the group velocity as we will see later.

Property	Crystal Fiber \ Erlangen
Dispersion D_0	$28 \setminus 36\,\mathrm{ps/(nm\,km)}$
Dispersion D_m	$-150 \setminus -180\,\mathrm{ps/(nm\,km)}$
Third order dispersion $dD_m/d\lambda$	$-0.6 \setminus -0.75\,\mathrm{ps/(nm^2 km)}$
Dispersion $\beta_2(\lambda_0)$	$-9.5 \setminus -12\,\mathrm{ps^2/km}$
Dispersion $\beta_2(\lambda_m)$	$180 \setminus 210\,\mathrm{ps^2/km}$
Group velocity-matched wavelength λ_m	$1508 \setminus 1494\,\mathrm{nm}$
Birefringence $\Delta n_0 \setminus \Delta n_m$	$7.5 \setminus 5.7 \times 10^{-4}$
Nonlinearity γ (780 nm)	$0.1\,\mathrm{W^{-1}m^{-1}}$
Fiber length L	$1.5\,\mathrm{m}$

Table 1. Properties of fiber NL-PM-750B (Philbin et. al, 2008). Dispersion data according to Crystal Fiber \ Alexander Podlipensky & Philip Russell, Max Planck Research Group in Optics, Information and Photonics, Erlangen. Nonlinearity according to Crystal Fiber. The fiber birefringence Δn and length L were measured by the authors. The symbols are defined in the text.

7.2 Frequency shifts

Let us now consider the frequency shifts at a group velocity horizon. During the pulse-probe interaction, the co-moving frequency ω' is a conserved quantity and so the probe frequency ω follows a contour line of ω' as a function of the nonlinear susceptibility χ induced by the pulse, see Fig. 4. The maximal χ experienced by the probe is proportional to the peak susceptibility χ_0 experienced by the pulse: assuming perfect mode overlap of pulse and probe, $\chi_{\max}$ reaches $2\chi_0$ when the probe and the pulse are co-polarized and $2\chi_0/3$ when they are cross-polarized (Agrawal, 2001). If the pulse is a soliton, the peak susceptibility and dispersion are connected as (Agrawal, 2001)

$$\chi_0 = \frac{2n_0 c \lambda_0 D_0}{(\omega_0 T_0)^2} = \frac{2n_0 c |\beta_2(\lambda_0)|}{\omega_0 T_0^2} \tag{73}$$

where D_0 denotes the dispersion parameter at the carrier wavelength λ_0. For example, for a soliton at λ_0=800nm whose full width at half maximum (FWHM) is 70fs (corresponding to T_0=40fs), for n_0=1.5, D_m=30ps/(nmkm) the peak susceptibility χ_0 is 2×10^{-6}. Nevertheless, we show that this small variation in the optical properties is sufficient to generate a significant wavelength shift at the horizon.

We obtain the contours of ω' from the Doppler formula (33). We use relations (12) and (72), but integrate from the group velocity-matching point,
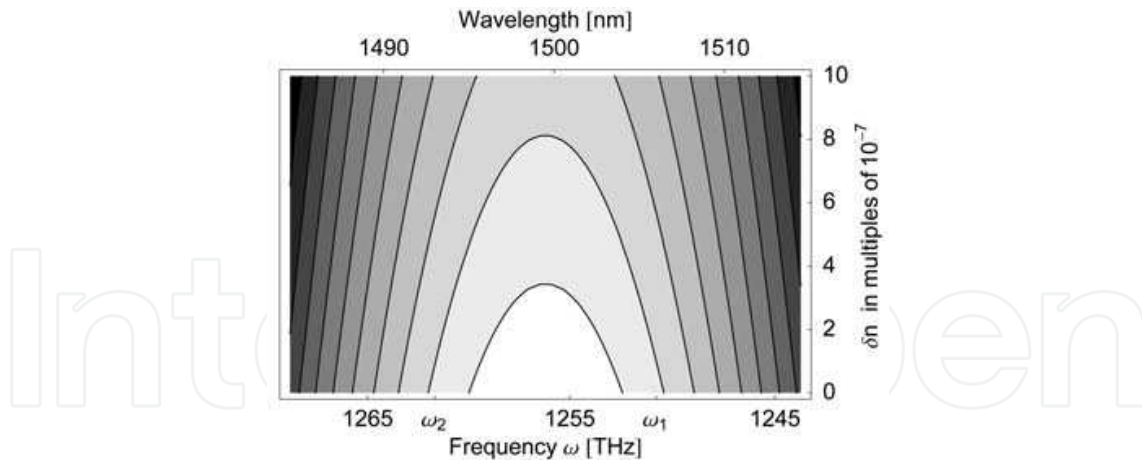
Fig. 4. Doppler contours. The pulse shifts the laboratory frequency ω (or the wavelength λ) of a probe along the contour line of constant ω' as a function (74) of the refractive-index change $\delta n = \chi/(2n_0)$. For a sufficiently intense pulse δn reaches the top of a contour. In this case the probe light completes an arch on the diagram while leaving the pulse; it is red- or blue-shifted, depending on its initial frequency (Philbin et. al, 2008).

$$
\begin{aligned}
\omega' &= \omega'_m - u \int_{\omega_m}^{\omega} \int_{\omega_m}^{\omega} \beta_2 \, d\omega \, d\omega - \frac{\chi}{2n_0} \frac{u}{c} \omega \\
&\approx \omega'_m - \frac{u}{2} \beta_2(\omega_m)(\omega - \omega_m)^2 - \frac{\chi}{2n_0} \frac{u}{c} \omega_m
\end{aligned}
\tag{74}
$$

$$
\approx \omega'_m + \frac{\pi u}{\lambda_m}\left(\frac{D_m c(\lambda - \lambda_m)^2}{\lambda_m} - \frac{\chi}{n_0} \right).
\tag{75}
$$

The contours of ω' do not depend on ω'_m nor on the scaling factor $\pi u/\lambda_m$. Because $D_m = D(\lambda_m)$ < 0, they form inverted parabolas with a maximum at λ_m for the corresponding $\chi_{\max}$. They intersect the axis of zero χ at the incident and the emerging wavelengths. Here $|D_m| c(\lambda - \lambda_m)^2/\lambda_m$ equals $\chi_{\max}/n_0$, and so we get

$$
\lambda = \lambda_m \pm \delta\lambda, \quad \delta\lambda = \sqrt{\frac{\lambda_m \chi_{\max}}{|D_m| n_0 c}}.
\tag{76}
$$

Using again that the pulse is a soliton, we obtain

$$
\delta\lambda = \frac{\sqrt{2r}\,\lambda_0}{T_0 \sqrt{\omega_0 \omega_m}} \sqrt{\left|\frac{D_0}{D_m}\right|} = \frac{\sqrt{2r\lambda_m}\,\lambda_0}{T_0 \omega_m} \sqrt{\left|\frac{\beta_2(\lambda_0)}{\beta_2(\lambda_m)}\right|}
\tag{77}
$$

with $r=2$ for co-polarized and $r=2/3$ for cross-polarized pulse and probe light. According to Fig. 4 the probe light can maximally be wavelength-shifted from $+\delta\lambda$ to $-\delta\lambda$ over the range $2\delta\lambda$. For the soliton mentioned above the group velocity dispersion D_0 is about 30ps/(nmkm). Using $\lambda_m \approx 1500$nm and $D_m \approx -160$ps/(nmkm), the wavelength shift $2\delta\lambda$ is 20nm in the co-polarized case and $2\delta\lambda=12$nm in the cross-polarized case.

We also derive a simple estimate of the efficiency of the frequency shifting. The probe undergoes frequency conversion at the horizon. However, because the group velocities of

the probe v_g and of the pulse u are similar, only a small fraction of the total probe light can be converted within the finite length of the fiber. The pulse and the slightly faster probe light travel through the fiber in $t=L/u$ and $t_p=L/v_g$ with $t > t_p$. The time difference multiplied with the probe power P_{probe} is the energy E_{coll} converted by pulse collision: $E_{\text{coll}}=P_{\text{probe}} L(1/u - 1/v_g)$. Therefore, the fraction η of probe power that is frequency converted is

$$\eta = v_{\text{rep}} L \left(1/u - 1/v_g\right) \approx v_{\text{rep}} L |D_m| \delta\lambda, \tag{78}$$

where v_{rep} is the repetition rate of the pulses and $1/v_g=\partial\beta/\partial\omega\approx 1/u + D_m\delta\lambda$ was used. For $L=1.5$m and $v_{\text{rep}}=80$MHz the maximal conversion efficiency η is on the order of 10^{-4}. Note that this model assumes that all of the probe light that interacts with the pulse is frequency shifted. However, in reality this rate can be lower due to the effect of tunnelling of probe light through the pulse.

7.3 Experimental results

The experiment is arranged as displayed in Fig. 5. A modelocked Ti:Sapphire laser (Mai Tai, Spectra Physics) delivers 70-fs pulses (FWHM) in the near infrared (NIR) at 80MHz repetition rate. These linearly polarized pulses are coupled to either one of the principal axes of the microstructured fiber of length $L=1.5$m. The polarization is rotated by a half-wave plate. Note that the polarizing beam splitter (PBS) only acts on the probe light. At the fiber output temporal autocorrelation traces and spectra are taken to determine the pulse energy necessary to create a fundamental soliton. For the center wavelength of 803nm, a dispersion $D_0=30$ps/(nmkm) and a nonlinearity γ of 0.1W^{-1}m^{-1}, 70-fs solitons are generated at 5pJ pulse energy corresponding to 400μW average power for the repetition rate $v_{\text{rep}} = 80$MHz.
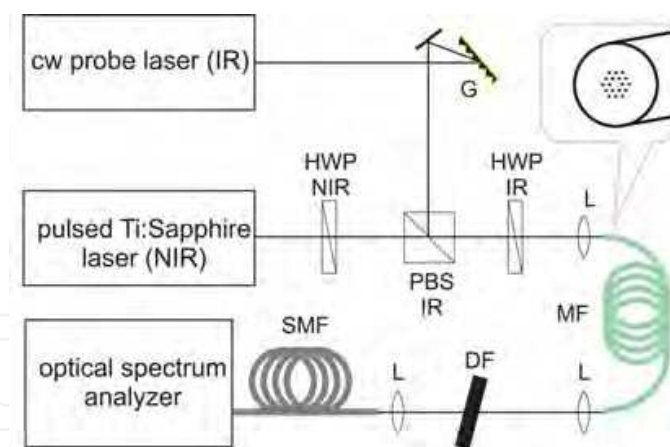

Fig. 5. Light from a continuous infrared (IR) laser is filtered by a diffraction grating (G) and is steered into a microstructured fiber (MF) by a polarizing beam splitter (PBS), a half wave plate (HWP), and a coupling lens (L). Near-infrared (NIR) pulses are launched as well. After the fiber the pulses are removed by a dichroic filter (DF) and the probe spectrum is taken through a standard single mode fiber (SMF) (Philbin et. al, 2008).

The output pulse length equalled the 70-fs input pulse length at an input power of approximately 320μW. This indicates that a soliton has formed. The observed power in comparison with the predicted power of 400μW illustrates the uncertainty in the actual fiber dispersion and nonlinearity. The observed Raman-induced soliton self-frequency shift

(Agrawal, 2001; Mitschke & Mollenauer, 1986; Gordon, 1986) was $\lesssim$ 4nm. Note that this shift decelerates the pulse and hence is changing the group velocity-matched wavelength λ_m in the infrared (IR). To calculate how much λ_m is shifted, we use Eq. (71), replacing λ_0 and λ with $\lambda_0 + \delta\lambda_0$ and $\lambda_m + \delta\lambda_r$ and linearize. In this way we get

$$\delta\lambda_r = \frac{D_0}{D_m}\delta\lambda_0. \tag{79}$$

For the dispersion data shown in Fig. 3, a wavelength change of 4nm of the pulse changes λ_m by $\delta\lambda_r = -0.75$nm. Since the probe light is wavelength-shifted symmetrically around λ_m, there is a change of the wavelength shift of up to -1.5nm.

The probe light is derived from a tunable external grating diode laser (Lynx Series, Sacher Lasertechnik). It delivers up to 20mW of continuous-wave light, tunable from 1460 to 1540nm. The probe light is reflected off a diffraction grating to reduce fluorescence emitted near lasing bandwidth. With another half-wave plate the probe light is coupled into the fiber onto one of the principal axes. Depending on wavelength, 100 to 600μW of probe power were coupled through the fiber. After the fiber we use a dichroic optic to filter out all of the pulse light and couple the IR light into a single-mode fiber connected to an optical spectrum analyzer.
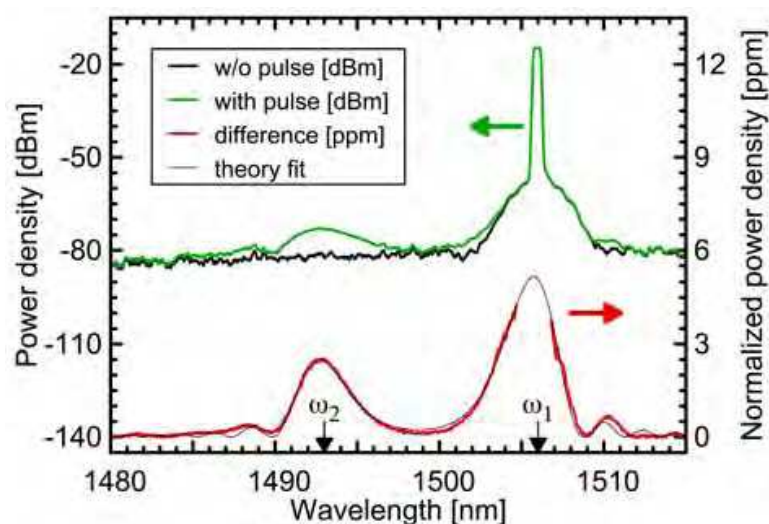
Fig. 6. Measurement of blue-shifting at a white-hole horizon (Philbin et. al, 2008). Spectrum of the blue-shifted light for a copolarized input probe of $\lambda = 1506$nm. Traces with (green) and without (black) pulses are shown on the logarithmic scale. Their difference is the normalized signal on the linear scale (red). The peak at ω_2 is the blue-shifted wave.

Figure 6 shows a typical output spectrum. This spectrum was taken with pulse and probe aligned to the slow axis of the fiber. At $\lambda=1506$nm the diode-laser input line is visible as a strong signal. From $\lambda=1502$nm to $\lambda=1510$nm we detect residual weak spontaneous emission from the laser that was not completely eliminated by the diffraction grating. Traces with and without pulses present in the fiber are taken and subtracted, leading to the signal displayed on a linear scale (red color). The signal is normalized by the amount of probe power and by the resolution bandwidth of 0.5nm. With the pulses present, a clear peak appears on the blue side of the input probe light near 1493nm. Since the blue-shifted light is generated from the part of the probe light that overlapped with the pulse during fiber propagation, it constitutes itself a pulse of finite length. Hence, this length is determined by the relative

group velocity of probe light and the pulse, see for example Eq. (78). In turn, the unshifted probe light is partially depleted, forming a gap in intensity. These features lead to a spectral broadening of both the shifted and unshifted probe light by a few nanometers. The spectra display clearly the blueshifting of waves as predicted by the theory of optical event horizons. In what follows we look at the influence of probe detuning as well as polarization changes, before we perform a direct fit of the spectrum in Fig.6 to the theory.

From the measurements shown in Fig. 6, the efficiency of the blue-shifting is 1.1×10^{-5}, less than the estimated 10^{-4}. This indicates that a significant part of the probe light tunnels through the pulse; the pulse is too short /weak to establish a nearly perfect barrier. In the tunneling region of the pulse the laboratory frequency $\omega - \omega_m$ is imaginary. In order to estimate the maximal imaginary part of ω we consider the extreme case where the initial frequency of the probe reaches the group velocity-matched frequency ω_m characterized by $\omega = \omega_m'$. We solve Eq. (74) for ω and obtain

$$\mathrm{Im}\omega = \sqrt{\frac{\chi \omega_m}{n_0 \beta_2(\omega_m)c}} = \frac{\sqrt{\chi}\,\omega_m}{\sqrt{n_0 c \lambda_m |D_m|}}. \tag{80}$$

Assuming $\chi \approx 2 \times 10^{-6}$ at the soliton peak, $n_0 \approx 1.5$, $\lambda_m = 1500$nm and $D_m = -160$ps/(nmkm) the imaginary part of ω reaches about 5THz. This is insufficient to significantly suppress tunnelling through a 70-fs pulse, because the product of $\mathrm{Im}\omega$ and T_0 is much smaller than unity. For longer or more intense pulses we expect perfectly efficient frequency conversion at the horizon.

Increasing the probe wavelength further away from λ_m is shifting light further to the blue side of the spectrum, because the wavelength shifts symmetrically around the group velocity-matched wavelength, according to Eq. (76) and Fig. 4. Figure 7 displays the spectra of shifted light for three detunings of the probe light from the group velocity-matched wavelength λ_m. As expected, the spectra move towards shorter wavelengths by the same amount as the probe laser was tuned towards longer wavelengths.

We also measured how the signal strength, the spectrum integrated over the signal peak, evolves with increasing probe power (Philbin et. al, 2008). A clear linear dependence was found in agreement with our theoretical model. This measurement proves that the probe indeed is a probe, not influencing the pulses via nonlinear effects.

Changing the input polarizations changes the group velocities of pulse and probe and therefore the group velocity-matched wavelength λ_m shifts by an amount $\delta\lambda_m$. If we change for example the pump polarization from the fast to the slow axis, the inverse group velocity $\beta_1(\lambda_0)$ increases as n_{g0}/c is replaced by $(n_{g0} + \Delta n_0)/c$. To maintain group velocity matching, $\beta_1(\lambda_m)$ has to change accordingly by $\Delta n_0/c$. We use Eq. (71), linearizing around λ_m, and get

$$\Delta n_0/c \approx D_m \delta\lambda_m. \tag{81}$$

For $D_m = -160$ps/(nmkm) and $\Delta n_0 = 7.5 \times 10^{-4}$ we obtain $\delta\lambda_m \approx -16$nm $\approx 2\delta\lambda$. This means that the polarization change induces a velocity change that is too large to maintain the optical horizon. Therefore, when changing polarizations, the probe laser has to be retuned to a wavelength were frequency shifting can be observed.

Figure 8 shows spectra for all four different polarization combinations. As expected, the group velocity-matched wavelength changes. Note that there also is a difference in λ_m for the two co-polarized cases, indicating small changes in the dispersion profile for the two polarization axes, a dispersion of the birefringence.
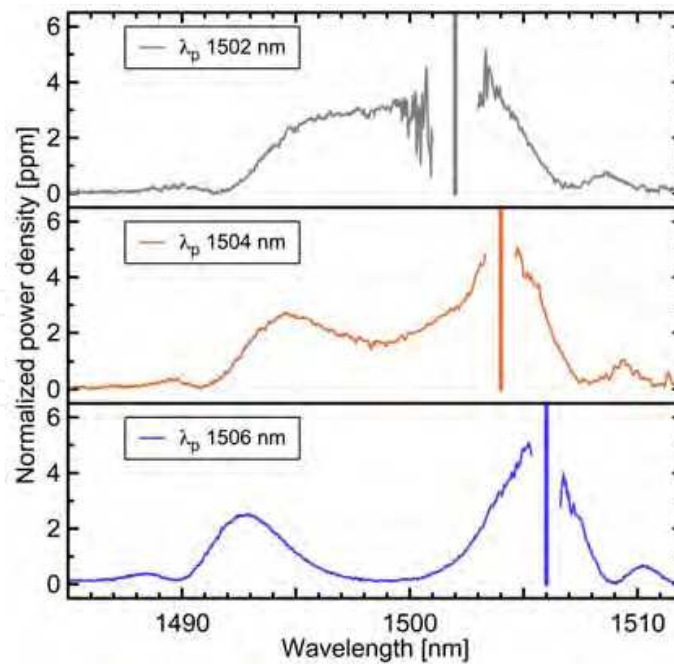
Fig. 7. Spectra for different input probe wavelengths. Since the probe mode is mirrored around the group velocity-matched wavelength λ_m, increasing probe wavelengths experience increasing blue shifting, as is also illustrated by the contours of Fig. 4 (Philbin et. al, 2008).
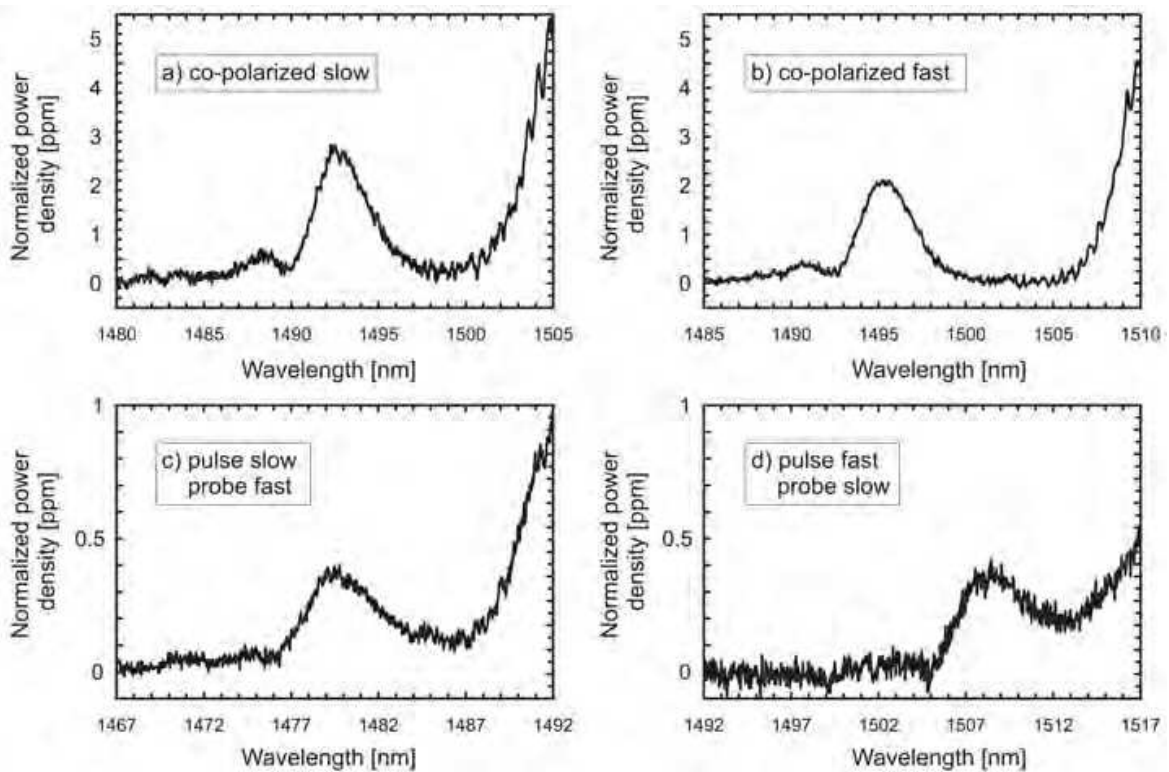

Fig. 8. Blue-shifted spectra for all four polarization combinations. Co-polarized spectra on the slow and fast axis in (a) and (b) and cross-polarized spectra with pulses slow (c) and fast (d). Group velocity-matched wavelengths are (a) 1499.5nm (b) 1503.2nm (c) 1486.4nm and (d) 1513.3nm (Philbin et. al, 2008).

7.4 Theoretical curve fitting of spectra

With the theory at hand, a functional expression for the spectra of the frequency-shifted probe light can be found. For brevity we are giving the results, the full calculation can be found in (Philbin et. al, 2008). The Fourier component of the shifted probe field is given by:

$$
\tilde{A}_s = \frac{\eta_r \mathcal{A}_0}{\pi(\omega + \omega_s - 2\omega_m)} \left[\exp\left(iq(\omega - \omega_m)^2\right) - \exp\left(iq(\omega_s - \omega_m)^2\right) \right]
$$
$$
- \frac{\mathcal{A}_0}{\pi(\omega - \omega_s)} \left[G\left(\sqrt{-iq}(\omega - \omega_m)\right) - G\left(\sqrt{-iq}(\omega_s - \omega_m)\right) \right] .,
$$

(82)

Here $\mathcal{A}_0$ is the overall amplitude, ω_s is the shifted probe frequency, η_r is a phenomenological inclusion of the soliton self-frequency shift (Mitschke & Mollenauer, 1986; Gordon, 1986) in terms of a reduced blue-shifted part of the spectrum. The parameter $q = \pi c |D_m| L / \omega_m^2$ combines the experimental parameters fiber length L, dispersion D_m, and group velocity-matched frequency ω_m. Finally, $G(x) = \int_{-\infty}^{+\infty} e^{-\xi^2} / \pi(x - \xi) d\xi$. The power spectrum measured corresponds to $|\tilde{A}|^2$.

Figure 6 also shows the fit of the observed spectrum with the theoretical curve (82). As fitting parameters we used the overall amplitude $\mathcal{A}_0$, the shifted probe frequency ω_s and group velocity-matched frequency ω_m, the dispersion D_m and η_r. We obtain a very good fit for $\mathcal{A}_0 = 4.1 \times 10^{12} \sqrt{W}s$, $\lambda_s = 1505.31$nm, $\lambda_m = 1499.38$nm, $D_m = -187$ps/(nmkm) and $\eta_r = 0.80$. The shift in λ_p to λ_s is consistent with the effect (79) of the soliton self-frequency shift. The fitted values for D_m and λ_m agree with the independently measured dispersion and the group velocity-matched frequency calculated from the dispersion curve of Fig. 3.

8. Conclusion

In conclusion, we have developed a theory for artificial event horizons in fibers. Experimentally, light was blue-shifted by a near group velocity-matched pulse. The measured data was explained by the presence of an optical group velocity horizon inside the fiber. A very good agreement between theory and experiment was observed. The blue shifting corresponds to the optical analogue of trans-Planckian frequency shifts in astrophysics (t'Hooft, 1985; Jacobson, 1991). The temperature of analogue Hawking radiation was calculated to show that the system gives a realistic chance for experimental observation. In this way, we have demonstrated classical optical effects of the event horizon in our analogue system, a first step towards tabletop astrophysics (Ball, 2001).

Aside from the prospect of analogue Hawking radiation, the group velocity horizons could be used for ultrafast delay lines, dispersion management, frequency conjugation, or quantum frequency conversion.

9. References

M. J. Ablowitz and A. S. Fokas (1997). *Complex Variables* (Cambridge University Press, Cambridge, 1997).

G. Agrawal (2001). *Nonlinear Fiber Optics* (Academic Press, San Diego, 2001).

P. Ball (2001). Nature 411, 628.

S. M. Barnett and S. J. D. Phoenix (1989). Phys. Rev. A 40, 2404.

S. M. Barnett and S. J. D. Phoenix (1991). Phys. Rev. A 44, 535.

G. Barton and C. Eberlein (1993). Ann. Phys. (New York) 227, 222.

J. D. Bekenstein (1973). Phys. Rev. D 7, 2333; see also arXiv:gr-qc/0009019 for a review.

N. D. Birrell and P. C. W. Davies (1984). *Quantum fields in curved space* (Cambridge University Press, Cambridge, 1984).

M. Born and E. Wolf (1999). *Principles of Optics* (Cambridge University Press, Cambridge, 1999).

T. Brabez and F. Krausz (2000). Rev. Mod. Phys. 72, 545.

N. G. R. Broderick, D. Taverner, D. J. Richardson, M. Ibsen, and R. I. Laming (1997). Phys. Rev. Lett. 79, 4566.

R. Brout, S. Massar, R. Parentani, and Ph. Spindel (1995) (a)., Phys. Rep. 260, 329.

R. Brout, S. Massar, R. Parentani, and Ph. Spindel (1995) (b). Phys. Rev. D 52, 4559.

C. M. Caves (1982). Phys. Rev. D 26, 1817.

S. Corley and T. Jacobson (1999). Phys. Rev. D 59, 124011.

P. C.W. Davies (1975). J. Phys. A 8, 609.

F. DeMartini, C. H. Townes, T. K. Gustafson, and P. L. Kelley (1967). Phys. Rev. 167, 312.

C. N. de Sterke (1992). Opt. Lett. 17, 914.

B. S. DeWitt (1975). Phys. Rep. 19, 295.

A. Efimov, A.V. Yulin, D.V. Skryabin, J. C. Knight, N. Joly, F. G. Omenetto, A. J. Taylor, and P. Russe (2005). Phys. Rev. Lett. 95, 213902.

D. Faccio1, S. Cacciatori, V. Gorini, V.G. Sala, A. Averchi, A. Lotti, M. Kolesik, J.V. Moloney (2009). arXiv:0905.4426v1 [gr-qc] 27 May 2009.

S. A. Fulling (1973). Phys. Rev. D 7, 2850.

L. J. Garay, J. R. Anglin, J. I. Cirac, and P. Zoller (2000). Phys. Rev. Lett. 85, 4643.

S. Giovanazzi, C. Farrell, T. Kiss, and U. Leonhardt (2004). Phys. Rev. A 70, 063602.

S. Giovanazzi (2005). Phys. Rev. Lett. 94, 061302.

A. V. Gorbach and D. V. Skryabin (2007). Nature Photonics 1, 653.

J. P. Gordon (1986). *ibid.* 11, 662.

M. B. Green, J. H. Schwarz, and E. Witten (1987). *Superstring Theory* (Cambridge University Press, Cambridge, 1987).

A. Hasegawa and F. Tappert (1973). Appl. Phys. Lett. 23, 142.

S. M. Hawking (1974). Nature 248, 30.

S. M. Hawking (1975). Commun. Math. Phys. 43, 199.

S. Hill, C. E. Kuklewicz, U. Leonhardt, and F. Knig (2009). Opt. Express, 17 13588.

T. Jacobson (1991). Phys. Rev. D 44, 1731.

T. A. Jacobson and G. E. Volovik (1998). Phys. Rev. D 58, 064021.

Few-Cycle Laser Pulse Generation and Its Applications, edited by F. X. Kärtner (Springer, Berlin, 2004).

J. C. Knight, T. A. Birks, P. S. Russell, and D. M. Atkin (1996). Opt. Lett. 21, 1547; P. Russell (2003). Science 299, 358.

See e.g. L. Knöll, S. Scheel, and D.-G.Welsch (2001). *QED in dispersing and absorbing media*, in *Coherence and Statistics of Photons and Atoms* ed. by J. Perina (Wiley, New York, 2001), pp.1-63.

L. D. Landau and E. M. Lifshitz (1975). The Classical Theory of Fields (Pergamon, Oxford, 1975).

L. D. Landau and E. M. Lifshitz (1976). *Mechanics* (Pergamon, Oxford, 1976).

L. D. Landau and E. M. Lifshitz (1977). *Quantum Mechanics* (Pergamon, Oxford, 1977).

L. D. Landau and E. M. Lifshitz (1984). *Electrodynamics of Continuous Media* (Pergamon, Oxford, 1984).

See e.g. U. Leonhardt (1993). *Quantum Theory of Simple Optical Instruments*, PhD thesis, Humboldt University Berlin.

U. Leonhardt, M. Munroe, T. Kiss, Th. Richter, and M. G. Raymer (1996), Opt. Commun. 127, 144.

U. Leonhardt and P. Piwnicki (2000). Phys. Rev. Lett. 84, 822.

U. Leonhardt (2002). Nature 415, 406.

U. Leonhardt (2003). Rep. Prog. Phys. 66, 1207.

U. Leonhardt and T. G. Philbin (2006). New J. Phys. 8, 247.

U. Leonhardt and T. G. Philbin (2007). *Black-hole lasers revisited*, in *Quantum Analogues: From Phase Transitions to Black Holes and Cosmology* edited by W. G. Unruh and R. Schützhold (Springer, Berlin, 2007).

L. Mandel and E. Wolf (1995). *Optical Coherence and Quantum Optics*, (Cambridge University Press, Cambridge, 1995).

R. Meinel, G. Neugebauer, and H. Steudel (1991). *Solitonen* (Akademie Verlag, Berlin, 1991).

P. W. Milonni (1994). *The Quantum Vacuum: An Introduction to Quantum Electrodynamics* (Academic Press, San Diego, 1994).

P. W. Milonni (2004). *Fast Light, Slow Light and Left Handed Light* (Institute of Physics, Bristol, 2004).

F. M. Mitschke and L. F. Mollenauer (1986). Opt. Lett. 11, 659.

L. F. Mollenauer, R. H. Stolen, and J. P. Gordon (1980), Phys. Rev. Lett. 45, 1095.

G. Moore (1970). J. Math. Phys. 11, 2679.

Any two-dimensional Riemannian manifold is conformally flat, see M. Nakahara (2003). *Geometry, Topology and Physics* (Institute of Physics, Bristol, 2003), Sec. 7.6.

N. Nishizawa and T. Goto (2002). Opt. Lett. 27, 152.

(2002). *Artificial black holes*, edited by M. Novello, M. Visser, and G. E. Volovik (World Scientific, Singapore, 2002).

T. G. Philbin, C. Kuklewicz, S. Robertson, S. Hill, F. König, and U. Leonhardt (2008). Science 319, 1367.

W. H. Reeves, D. V. Skryabin, F. Biancalana, J. C. Knight, P. S. Russell, F. G. Omenetto, A. Efimov, and A. J. Taylor (2003). Nature 424, 511.

G. Rousseaux, C. Mathis, P. Maïssa, T. G. Philbin, and U. Leonhardt (2008). New J. Phys. 10, 053015.

C. Rovelli (1998). Living Rev. Rel. 1, 1.

P. Russell (2003). Science 299, 358.

W. Schleich and M. O. Scully (1984). in *New trends in atomic physics*, edited by G. Grynberg and A. Stora, (Les Houches, Session XXXVIII, 1982, Elsevier Science Publishers B. V.)

R. Schützhold and W. G. Unruh (2002). Phys. Rev. D 66, 044019.

R. Schützhold and W. G. Unruh (2005). Phys. Rev. Lett. 95, 031301.

J. Schwinger (1951). Phys. Rev. 82, 664.

M. J. Steel, D. G. A. Jackson, and S. M. de Sterke (1994), Phys. Rev. A 50, 3447.

G. t'Hooft (1985). Nucl. Phys. B 256, 727.

J. S. Toll (1956). Phys. Rev. 104, 1760.

W. G. Unruh (1976). Phys. Rev. D 14, 870.

W. G. Unruh (1981). Phys. Rev. Lett. 46, 1351.

W. G. Unruh (1995). Phys. Rev. D 51, 2827.

M. Visser (1998). Class. Quantum Grav. 15, 1767.

G. E. Volovik (2002). JETP Lett. 76, 240.

G. E. Volovik (2003). *The Universe in a Helium Droplet* (Clarendon Press, Oxford, 2003).

S. Weinberg (1999). *The Quantum Theory of Fields* (Cambridge University Press, Cambridge, 1999), Volume I.
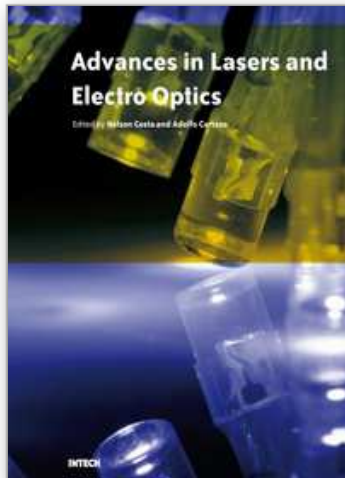
Advances in Lasers and Electro Optics

Edited by Nelson Costa and Adolfo Cartaxo

Lasers and electro-optics is a field of research leading to constant breakthroughs. Indeed, tremendous advances have occurred in optical components and systems since the invention of laser in the late 50s, with applications in almost every imaginable field of science including control, astronomy, medicine, communications, measurements, etc. If we focus on lasers, for example, we find applications in quite different areas. We find lasers, for instance, in industry, emitting power level of several tens of kilowatts for welding and cutting; in medical applications, emitting power levels from few milliwatt to tens of Watt for various types of surgeries; and in optical fibre telecommunication systems, emitting power levels of the order of one milliwatt. This book is divided in four sections. The book presents several physical effects and properties of materials used in lasers and electro-optics in the first chapter and, in the three remaining chapters, applications of lasers and electro-optics in three different areas are presented.

How to reference

In order to correctly reference this scholarly work, feel free to copy and paste the following:

Friedrich Konig, Thomas G. Philbin, Chris Kuklewicz, Scott Robertson, Stephen Hill and Ulf Leonhardt (2010). Analogue of the Event Horizon in Fibers, Advances in Lasers and Electro Optics, Nelson Costa and Adolfo Cartaxo (Ed.), ISBN: 978-953-307-088-9, InTech, Available from: http://www.intechopen.com/books/advances-in-lasers-and-electro-optics/analogue-of-the-event-horizon-in-fibers

INTECH
open science | open minds